Energy Conversion and Management 86 (2014) 670–682

Contents lists available at ScienceDirect

Energy Conversion and Management

journal homepage: www.elsevier.com/locate/enconman

Numerical simulations for the coal/oxidant distribution effects between two-stages for multi opposite burners (MOB) gasifier

Imran Nazir Unar [a,*], Lijun Wang [b,*], Abdul Ghani Pathan [c], Rasool Bux Mahar [d], Rundong Li [b], M. Aslam Uqaili [e]

[a] Department of Chemical Engineering, MUET Jamshoro, Pakistan
[b] School of Energy and Environment, Shenyang Aerospace University, China
[c] Department of Mining Engineering, MUET Jamshoro, Pakistan
[d] Department of Environmental Engineering, MUET Jamshoro, Pakistan
[e] Department of Electrical Engineering, MUET Jamshoro, Pakistan

ARTICLE INFO

Article history:
Received 15 February 2014
Accepted 10 June 2014
Available online 2 July 2014

Keywords:
Multi opposite burners (MOB)
Coal gasification
Entrained flow gasifier
Coal/oxidant distribution

ABSTRACT

A 3D CFD model for two-stage entrained flow dry feed coal gasifier with multi opposite burners (MOB) has been developed in this paper. At each stage two opposite nozzles are impinging whereas the two other opposite nozzles are slightly tangential. Various numerical simulations were carried out in standard CFD software to investigate the impacts of coal and oxidant distributions between the two stages of the gasifier. Chemical process was described by Finite Rate/Eddy Dissipation model. Heterogeneous and homogeneous reactions were defined using the published kinetic data and realizable k–ε turbulent model was used to solve the turbulence equations. Gas–solid interaction was defined by Euler–Lagrangian frame work. Different reaction mechanism were investigated first for the validation of the model from published experimental results. Then further investigations were made through the validated model for important parameters like species concentrations in syngas, char conversion, maximum inside temperature and syngas exit temperature. The analysis of the results from various simulated cases shows that coal/oxidant distribution between the stages has great influence on the overall performance of gasifier. The maximum char conversion was found 99.79% with coal 60% and oxygen 50% of upper level of injection. The minimum char conversion was observed 95.45% at 30% coal with 40% oxygen at same level. In general with oxygen and coal above or equal to 50% of total at upper injection level has shown an optimized performance.

1. Introduction

Depletion of conventional energy resources like fossil fuels have diverted the focus of engineers and researchers, around the globe, to develop the energy efficient systems particularly for industries. Advancements of new economic and efficient technologies like co-generation [1], combined cycles [2,3] and gasification [4] are one of the prime concern, nowadays for developing countries to meet the socio-economic sustainability. Coal gasification is a complex process in which fuel is converted to combustible gases (CO and H_2) in the presence of water and oxygen, at elevated pressures and temperatures. Product gas is known as "syngas" which can be used as town gas, to make electric power, methanol, liquid fuels, urea, ammonia, etc. [5]. Coal gasification is highly environment friendly as it has the capability to achieve extremely low SO_x, NO_x and particulate emissions [6].

For a successful and efficient coal gasification, a deep understanding of all physical and chemical changes involved in the process, is required. Numerical simulation provides an easy, cost effective and reliable way, to study the effect of various controlling parameters, like coal composition, oxidant to fuel ratio, residence time of fuel particles in the system, temperature and pressure of the gasifier, rate of chemical reactions, etc. on the gasification process. For last 20 years, the CFD modeling remained an effective tool to simulate and visualize the gasification process [7–12]. Different mathematical models have been developed for various sub-processes involved in the coal gasification. For instance some researchers have developed Euler–Euler model to define the gas and solid flows [6,13–16] whereas, the others have used Euler–Lagrangian frame work to setup the gas and solid interactions [17–20]. Probability Density Functions (PDF) [10,21,22] model and Finite Rate Chemistry/Eddy Dissipation models [14,23–25]

* Corresponding authors.
E-mail addresses: imran.nazir@faculty.muet.edu.pk (I.N. Unar), wanglijun@sau.edu.cn (L. Wang).

http://dx.doi.org/10.1016/j.enconman.2014.06.028
0196-8904/

Nomenclature

ρ, ρ_p	density, density of particles (kg/m^3)
u, u_p	velocity, velocity of particles (m/s)
S_m, S_j, S_h, S_r	source terms for mass, momentum, energy and species
c_p	specific heat at constant pressure (J/kg K)
τ_{ij}	symmetric stress tensor
T	temperature (K)
λ	turbulent thermal conductivity (W/m K)
C_j	mole fraction of specie j
D_i	diffusivity (m^2/s)
F_D	drag force (kg m/s)
F_x	force vector component along x-axis (kg m/s^2)
μ	dynamic viscosity (N s/m^2)
k	kinetic energy for turbulence (m^2/s^2)
ε	dissipation rate of turbulence (m^2/s^3)
μ_t	turbulence viscosity
C_μ	viscosity constant
G_k	mean velocity gradients
D_t	diffusion coefficient for turbulence (m^2/s)
Pr_t	Prandtl number for turbulence
Sc_t	Schmidt number for turbulence
q_r	heat flux for radiation heat (J/m^2 s)
G	incident radiation
C	coefficient of function for linear-anisotropic phase
a	absorption coefficient
σ_s	scattering coefficient (m^{-1})
σ	Stefan–Boltzmann constant
ε_w	emissivity
$W_{j,r}$	net production rate of species i through chemical reaction (K mol/m^3 s)
M_j	molecular weight of specie j
$\nu''_{j,r}$	Stoichiometric coefficient for product j in reaction r
$\nu'_{i,r}$	Stoichiometric coefficient for reactant i in reaction r
[C]	molar concentration of specie (K mol/m^3)
η''	rate exponent for product specie
η'	rate exponent for product reactant specie
k_f	forward reaction rate constant
A	pre-exponential factor (consistent units)
B	temperature constant (dimensionless)
E_a	activation energy for reaction (J/K mol)
R	universal gas constant (J/K mol K)

are the most common methods, used so far, to define the chemistry of the gasification reactions.

The effects of major design and operating parameters like particle density/size, oxygen/coal ratio, injector nozzle design, number of nozzles, gasification reactions, etc., have been investigated by various researchers through CFD simulations [26–31]. Entrained flow gasifiers (EFSG) are considered to be the best in advanced integrated gasification combined cycle (IGCC) power plants, due to high carbon conversion efficiencies with short residence time [32]. Opposite Multi Burners (OMB) in entrained flow gasifiers are grown popular nowadays for the better fuel conversion due to high collision rates for solid particles and resolving the issues of deposition of slag/ash on gasifier walls [33–35]. In the OMB there are two sets of nozzles exactly opposite to each other which produce impinging flows. Tang et al. [36] has partially modified the design of OMB by changing one set of impinging nozzles into tangentially opposite to each other and he has introduced a second stage to develop flameless oxidation conditions. Two-stage entrained flow gasifier with impinging and tangential nozzles produces better results as compared to OMB gasifier with all impinging nozzles, but no study has been conducted, so far, to investigate the effects of fuel/oxidation amounts at each level on the overall performance of the gasifier.

The objective of present work is to study the effects of coal and oxidant distribution effects between two stages on important parameters of gasifier (like temperature and syngas composition, etc.) through numerical simulations. A 3D CFD model of two-stage coal gasifier with impinging and tangential nozzles is developed in which Euler–Lagrangian frame work and Finite Rate/Eddy Dissipation model are used. In the first part, few reaction mechanisms have been investigated to validate the model from experimental results. After the validation of the model the effects of coal and oxygen distribution have investigated with fixed oxygen/coal ratio on the performance of lignite coal gasifier.

2. Numerical method

2.1. Description of physical system

An oxygen-blown, entrained flow coal gasifier for Chinese high-ash lignite coal is used in this study as shown Fig. 1. The proximate and ultimate analysis of coal is listed in Table 1. The particle diameters are fitted to the Rosin–Rammler distribution (minimum dia is 4 μm, maximum dia is 125 μm, and mean dia 45.6 μm).

The inner radius of experimental gasifier is 0.32 m and its height is 0.55 m. The coal feeding rate is taken as 7.2 kg/h [37]. Four nozzles are installed at two levels of gasifier chamber named as AA′ Level (Top) and BB′ Level (Bottom). Two opposite nozzles, exactly at the central axis line for each levels, are impinging in nature whereas the other two nozzles are slightly at a side of the axis and produce a swirl in the flow and called tangential nozzles. At top (AA′ Level) the coal is injected with carrier inert gas (N_2) from opposite impinging nozzles whereas pure oxygen is injected through tangential nozzles. However at bottom (BB′ Level) the coal is injected with O_2 from impinging nozzles (Fig. 1). The amount of oxygen is calculated for all the cases on the basis of oxygen to coal (O/C) ratio with fixed coal feeding. The amount of coal and oxygen feedings at individual levels are calculated on the basis of selected coal or oxygen distribution at each level respectively.

2.2. Computational models

In present work, numerical study is carried out with 3D, steady and incompressible turbulence flow with heterogeneous and homogenous reactions. Therefore, time-averaged-steady-state Navier–Stokes, mass momentum and energy and species equations have solved. The governing equations for the system are as follows [5].

$$\frac{\partial}{\partial x_i}(\rho u_{ij}) = S_m \tag{1}$$

$$\frac{\partial}{\partial x_i}(\rho u_i u_j) = \rho \bar{g}_j - \frac{\partial P}{\partial x_i} + \frac{\partial}{\partial x_i}(\tau_{ij} - \rho\overline{u'_i u'_j}) + S_j \tag{2}$$

$$\frac{\partial}{\partial x_i}(\rho c_p u_i T) = \frac{\partial}{\partial x_i}\left(\lambda\frac{\partial T}{\partial x_i} - \rho c_p \overline{u'_i T'}\right) + \mu\Phi + S_h \tag{3}$$

$$\frac{\partial}{\partial x_i}(\rho u_i C_j) = \frac{\partial}{\partial x_i}\left(\rho D_i \frac{\partial C_j}{\partial x_i} - \rho\overline{u'_i C'_j}\right) + S_r \tag{4}$$

where τ_{ij} is the symmetric stress tensor and $\rho\overline{u'_i u'_j}$ is the Reynolds stress. The realizable k–ε turbulence model is also employed to

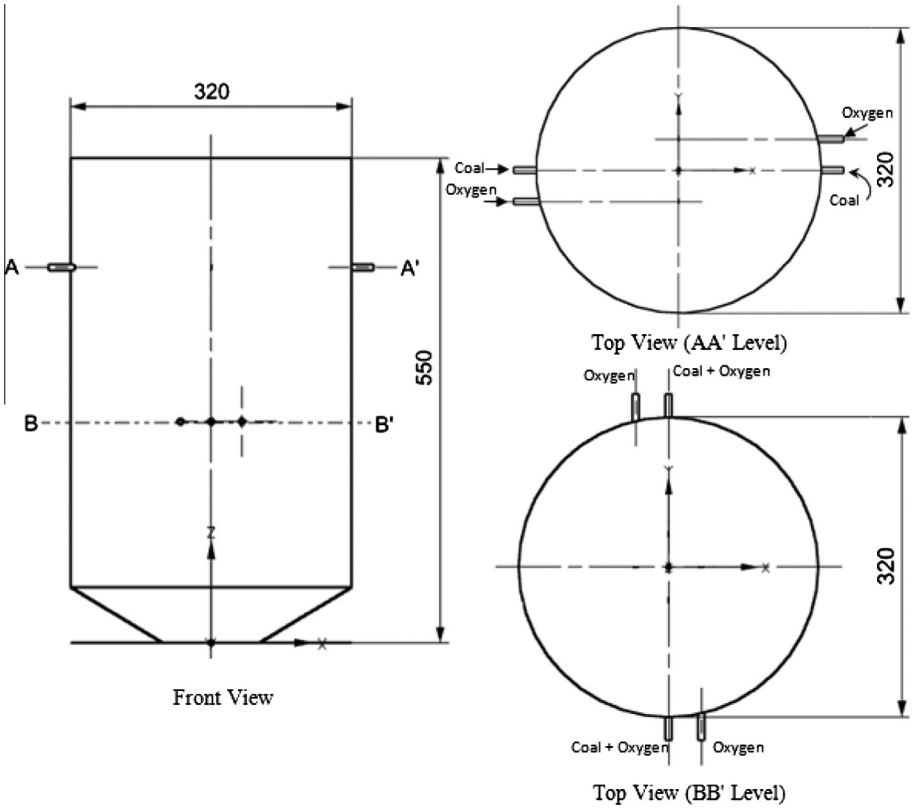

Fig. 1. (Left) Geometry of gasifier with main inlets and outlets. (Right) The sections of gasifier at AA′ and BB′ level.

Table 1
Properties of Chinese coal.

Proximate analysis (w/%)		Ultimate analysis (w_{ar}/%)	
Moisture	1.16	C	63.51
Ash	23.10	H	4.19
Volatile	27.03	O	6.39
Fixed carbon	48.21	N	1.02
		S	0.63
Heating value		32.91 MJ/kg	

Note: values are taken from earlier work [37].

solve the turbulent flow. The turbulence kinematic viscosity is calculated by:

$$\mu_t = \rho C_\mu k^2/\varepsilon \tag{5}$$

where C_μ is the viscosity constant, k the turbulence kinetic energy and ε the turbulence dissipation rate. k and ε are calculated from the following transport equations [38]:

$$\frac{\partial}{\partial x_i}(\rho u_i k) = \frac{\partial}{\partial x_i}\left[\left(\mu + \frac{\mu_t}{\sigma_k}\right)\frac{\partial k}{\partial x_i}\right] + G_k - \rho\varepsilon \tag{6}$$

$$\frac{\partial}{\partial x_i}(\rho u_i \varepsilon) = \frac{\partial}{\partial x_i}\left[\left(\mu + \frac{\mu_t}{\sigma_\varepsilon}\right)\frac{\partial \varepsilon}{\partial x_i}\right] + C_{1\varepsilon}G_k\frac{\varepsilon}{k} - C_{2\varepsilon}G_k\frac{\varepsilon^2}{k} \tag{7}$$

where G_k is the generation of turbulence kinetic energy due to mean velocity gradients. The constants in the transport equations are selected from Launder and Spalding [39] and they are given by C_μ = 0.09, $C_{1\varepsilon}$ = 1.44, $C_{2\varepsilon}$ = 1.92, σ_k = 1.0 and σ_ε = 1.3. The turbulence heat conductivity (λ) and diffusion coefficient (D) in Eqs. (3) and (4) are given by:

$$\rho c_p \overline{u_i' T'} = -\lambda\frac{\partial T}{\partial x_i} = c_p\frac{\mu_t}{\mathrm{Pr}_t}\frac{\partial T}{\partial x_i} \tag{8}$$

$$\rho\overline{u_i' C_j'} = -\rho D_i\frac{\partial C_j}{\partial x_i} = -\frac{\mu_t}{Sc_t}\frac{\partial C_j}{\partial x_i} \tag{9}$$

where Pr_t (=0.85) is the turbulence Prandtl number and Sc_t (=0.7) is the turbulence Schmidt number.

Lagrangian approach has been used to calculate the motion of particles by using Discrete Phase Model (DPM). The trajectories of coal particles are predicted in DPM by integrating the force balance on the coal particle, when they move through the continuous phase of the fluid [40]. This force balance equates the coal particle inertia with the forces acting on the coal particle, and can be written (for the x direction in Cartesian coordinates) as [41].

$$\frac{du_p}{dt} = F_D(u - u_p) + g_x\frac{\rho_p - \rho}{\rho_p} + F_x \tag{10}$$

The interaction between the discrete phase and the continuous phase is also taken into account by treating the heat and mass losses of the particles as the source terms in the governing equations.

P-1 model has adopted to calculate the radiant heat in the gasifier [9,10,13,41]. In P1 model, the local radiation intensity is calculated by the equation

$$-\nabla q_r = aG - 4aG\sigma T^4 \tag{11}$$

where

$$q_r = -\frac{1}{3(a+\sigma_s) - C\sigma_s}\nabla G \tag{12}$$

where a is the absorption coefficient, σ_s is the scattering coefficient, G is the incident radiation, C is the linear anisotropic phase function coefficient, and σ is the Stefan–Boltzmann constant.

2.3. Combustion/gasification model

Species transport model (Eq. (4)) is used for the gasification reactions chemistry. This modeling approach gives an option to define the important reactions and set their kinetic parameters. During the high temperature environment of coal gasification, the coal will be decomposed into volatiles, char and ash [42]. The compositions released from the coal can be expressed by the following equilibrium equation [43].

$$Coal \rightarrow \alpha_1\ Volatiles + \alpha_2\ H_2O + \alpha_3\ Char + \alpha_4\ Ash \quad (13)$$

After undergoing fast heating, the hot flow around coal particles will trigger a number of physical and chemical reactions [29]. The reactions include the devolatilization of coal, the combustion of volatiles and unburned char as well as the gasification of the char [44]. In present study, the volatiles are lumped into one volatile gas species $C_{1.37}H_{4.58}O_{0.44}$ and are calculated from proximate and ultimate analysis of coal. The volatiles release are described by a two-step devolatilization model [45] and it is given as follows:

$$Coal \xrightarrow{k_l} (1 - Y_l) \times Char_l + Y_l \times Volatile \quad (\text{for low temperature}) \quad (14)$$

$$Coal \xrightarrow{k_h} (1 - Y_h) \times Char_h + Y_h \times Volatile \quad (\text{for high temperature}) \quad (15)$$

where Y is stoichiometric coefficient. At low temperature Eq. (14) is dominated whereas Eq. (15) shows a higher rate at high temperature. The reaction kinetic equations are as follows:

$$\frac{dV}{dt} = (k_l Y_1 + k_h Y_h) Coal \quad (16)$$

$$k_l = A_l \exp(-E_l / RT_p) \quad (17)$$

$$k_h = A_h \exp(-E_h / RT_p) \quad (18)$$

where V denotes the mass fraction of volatiles, k is the reaction rate constant, A the pre-exponential factor, T_P the coal particle temperature and E the activation energy of the reaction. The values of Y_l, k_l, Y_h, k_h, E_l and E_h are obtained from previous studies which have been done on similar type of coal [45,46] and they are listed in Table 2.

When char is produced from coal devolatilization, CO and H_2 can be generated from char gasification. There are various reactions selected by different researchers to define the gasification reaction mechanism [5,6,13,14,17–20,23,25]. In this paper, preliminary simulations were carried out to find the best reaction mechanism among different reaction-sets. The details of those cases are tabulated in Table 2.

The various reaction mechanisms are modeled with following chemical species: C(s), O_2, N_2, CO, CO_2, H_2O, H_2 and volatiles. Finite Rate/Eddy Dissipation rate model has been used to calculate the rate of formation for each specie and update the source term S_r in Eq. (4) by the following expression.

$$S_r = M_j \sum_{j=1}^{N} w_{j,r} \quad (19)$$

$$w_{j,r} = (\upsilon''_{j,r} - \upsilon'_{j,r}) k_f \left(\prod_{i=1}^{N_r} [C]^{\eta''} - \frac{1}{K_{eq}} \prod_{i=1}^{N_r} [C]^{\eta''} \right) \quad (20)$$

$$k_f = A T^B e^{(-E_a/RT)} \quad (21)$$

In the above equation, the forward reaction rate constant k_f is established based on Arrhenius law; A is the pre-exponential factor, B the temperature exponent and E_a the activation energy of reaction. The values of A, B and E_a for various reactions are obtained from earlier studies and given in Table 3.

Table 2
Various preliminary cases to optimize the reaction mechanism.

Reactions	Simulation cases					
	A	B	C	D	E	F
Vol + 2.295 O_2 → 1.37 CO_2 + 2.29 H_2O (volatiles complete combustion)		✓	✓		✓	✓
Vol + 1.61 O_2 → 1.37 CO + 2.29 H_2O (volatiles partial combustion)		✓		✓		
C⟨s⟩ + 0.5 O_2 → CO (char partial combustion)	✓	✓	✓			✓
C⟨s⟩ + O_2 → CO_2 (char complete combustion)				✓	✓	✓
C⟨s⟩ + CO_2 → 2CO (gasification, Boudourad reaction)	✓	✓	✓	✓	✓	✓
C⟨s⟩ + H_2O → CO + H_2 (gasification)	✓	✓	✓	✓	✓	✓
CO + 0.5 O_2 → CO_2 (CO combustion)	✓					
H_2 + 0.5 O_2 → H_2O (H_2 combustion)	✓	✓	✓	✓	✓	✓
CO + H_2O ↔ CO_2 + H_2 (water gas shift reaction)	✓	✓	✓	✓	✓	✓

Table 3
Selected kinetic parameters for devolatilization and gasification/combustion reactions.

Devolatilization [45,46]			
Y_l; Y_h			0.3; 1
k_l; k_h (s^{-1})			2×10^5; 1.3×10^7
E_l; E_h (kJ mol^{-1})			104.6; 167.4
Combustion/gasification reactions [31]	A	B	E_a (J $K\ mol^{-1}$)
Heterogeneous reactions (solid–gas phase)			
C(s) + O_2 → CO_2	0.002	0	7.9×10^7
C(s) + 0.5O_2 → CO	0.052	0	6.1×10^7
C(s) + CO_2 → 2CO	242	0	2.75×10^8
C(s) + H_2O → CO + H_2	426	0	3.16×10^8
Homogeneous reaction (gas phase)			
CO + 0.5O_2 → CO_2	2.239×10^{12}	0	1.7×10^8
H_2 + 0.5 O_2 → H_2O	6.8×10^{15}	0	1.68×10^8
CO + H_2O ↔ CO_2 + H_2 (WGS reaction) f	2.75×10^{10}	0	8.38×10^7
b	2.65×10^{-2}	0	3.96×10^3
$C_{1.37}H_{4.58}O_{0.44}$ (volatile) + 1.61 O_2 → 1.37 CO + 2.29 H_2O (volatile partial combustion)	2.119×10^{11}	0	2.027×10^8
$C_{1.37}H_{4.58}O_{0.44}$ (volatile) + 2.295 O_2 → 1.37 CO_2 + 2.29 H_2O (volatile complete combustion)	2.119×10^{11}	0	2.199×10^{11}

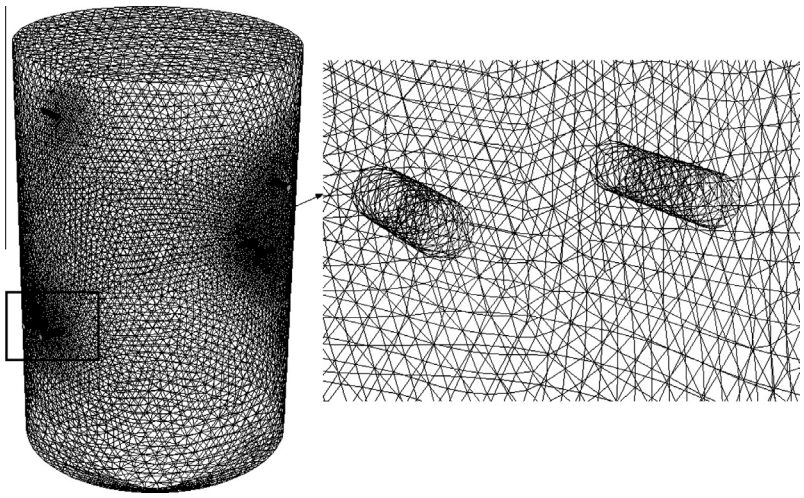

Fig. 2. Meshed geometry (left), closer view of bottom nozzles (right).

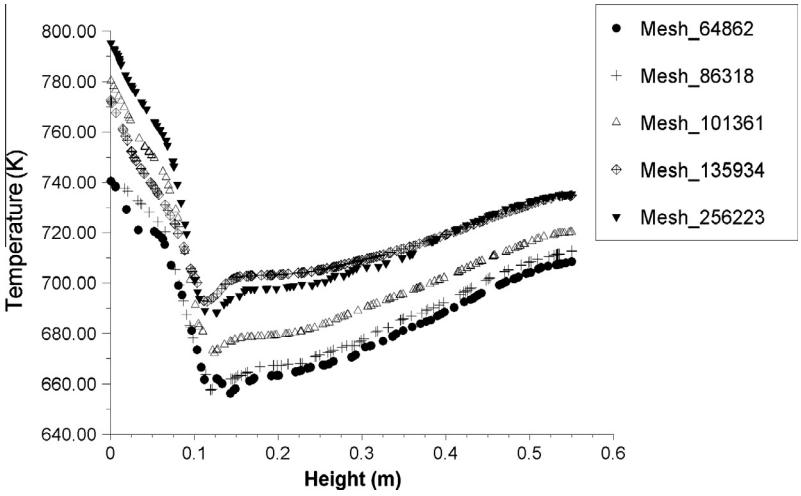

Fig. 3. Grid sensitivity study: temperature (K) distribution along height (m) for five grid sizes.

Table 4
Operated parameters for simulated cases.

Case name	1st Level (upper level, AA′-level)				2nd Level (down level, BB′-level)			
	Fraction of total coal (%)	Mass flow of coal (kg/s)	Fraction of total oxygen (%)	Mass flow of oxygen (kg/s)	Fraction of total coal (%)	Mass flow of coal (kg/s)	% Of total oxygen (%)	Fraction of total oxygen (kg/s)
C30_O40	30	0.0006	40	0.0008	70	0.0014	60	0.0012
C40_O40	40	0.0008	40	0.0008	60	0.0012	60	0.0012
C50_O40	50	0.001	40	0.0008	50	0.001	60	0.0012
C60_O40	60	0.0012	40	0.0008	40	0.0008	60	0.0012
C70_O40	70	0.0014	40	0.0008	30	0.0006	60	0.0012
C30_O50	30	0.0006	50	0.001	70	0.0014	50	0.001
C40_O50	40	0.0008	50	0.001	60	0.0012	50	0.001
C50_O50	50	0.001	50	0.001	50	0.001	50	0.001
C60_O50	60	0.0012	50	0.001	40	0.0008	50	0.001
C70_O50	70	0.0014	50	0.001	30	0.0006	50	0.001
C30_O60	30	0.0006	60	0.0012	70	0.0014	40	0.0008
C40_O60	40	0.0008	60	0.0012	60	0.0012	40	0.0008
C50_O60	*50*	*0.001*	*60*	*0.0012*	*50*	*0.001*	*40*	*0.0008*
C60_O60	60	0.0012	60	0.0012	40	0.0008	40	0.0008
C70_O60	70	0.0014	60	0.0012	30	0.0006	40	0.0008

Note: the case (C50_O60) is the case at original experimental conditions [37] and the results of that case will be used to validate the model.

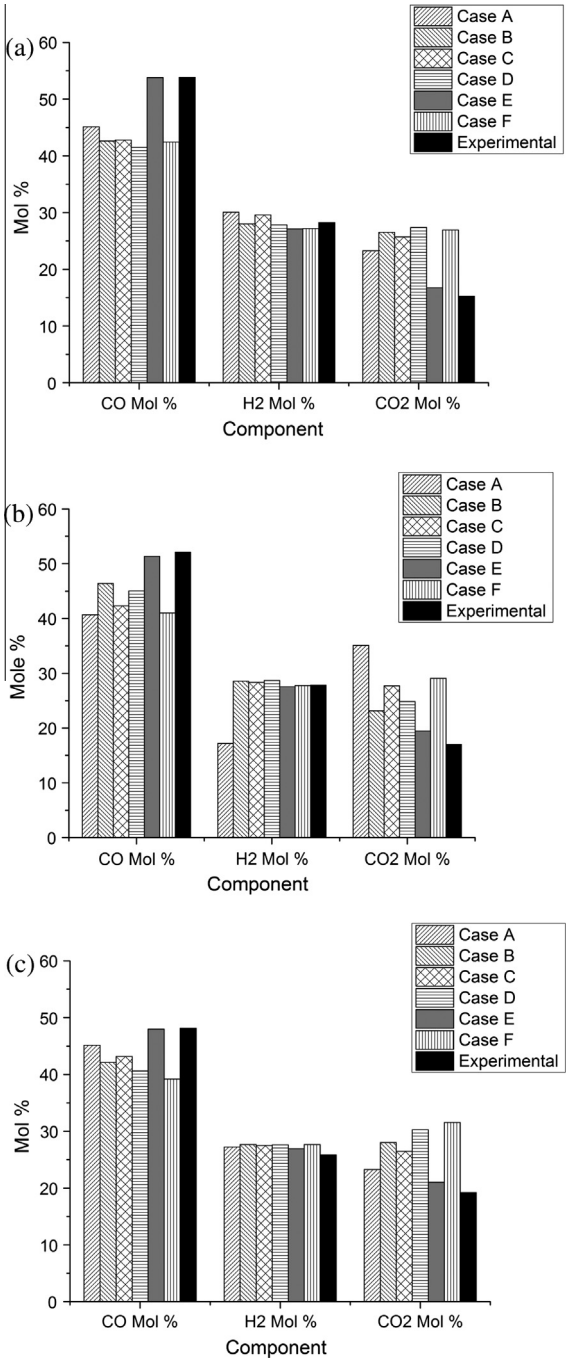

Fig. 4. The comparison of various preliminary simulation results with experimental values [37] for CO, H_2 and CO_2 mol fraction in syngas (a) at O/C ratio = 0.9, (b) at O/C ratio = 1.0 and (c) at O/C ratio = 1.1.

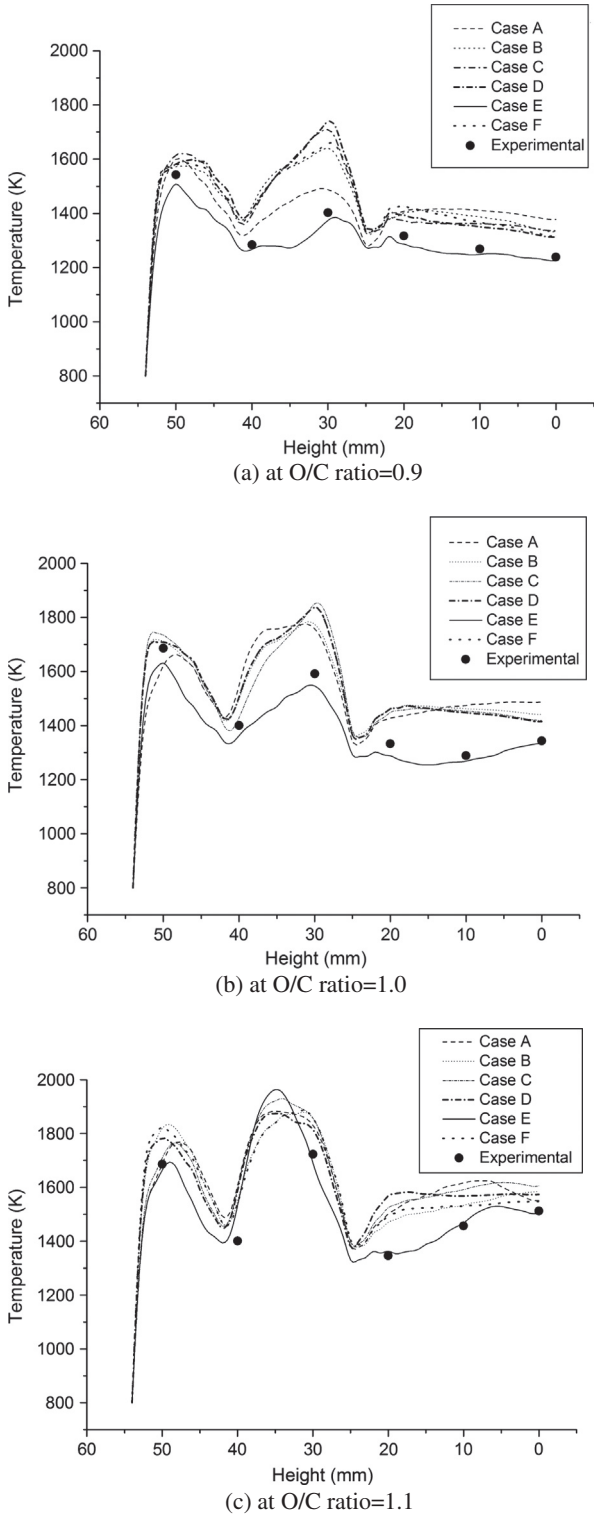

Fig. 5. The temperature profile for various preliminary simulated cases and experimental work along central axis of gasifier.

2.4. Boundary conditions and calculation methods

A 3D computational domain has developed with five different grid densities to analyze the grid sensitivity. Fig. 2 shows meshed domain along with the closer view of nozzles. Temperature is the most critical parameter in gasification so it was selected in grid sensitivity analysis. Cold flow simulations (no reaction) were carried out with all five different grids and temperature profile along the axis for all the grids are shown in Fig. 3. The grids with 135,934 and 256,223 tetrahedron cells shows almost same temperature distribution at the center line along height of gasifier. This shows that the solution is independent to the grid beyond 135,934 grid size hence this grid has selected for further calculations.

The mass-flow inlet and pressure-outlet boundary conditions were used for all input/output streams. Buoyancy force has considered in the present model. Water cooled walls were assumed to be at constant temperature at 800 K. No-slip state (zero velocity) is applied on the surfaces of walls. Steady-state simulations were carried out with an implicit pressure-correction scheme (pressure-based solver) by decoupling energy and momentum

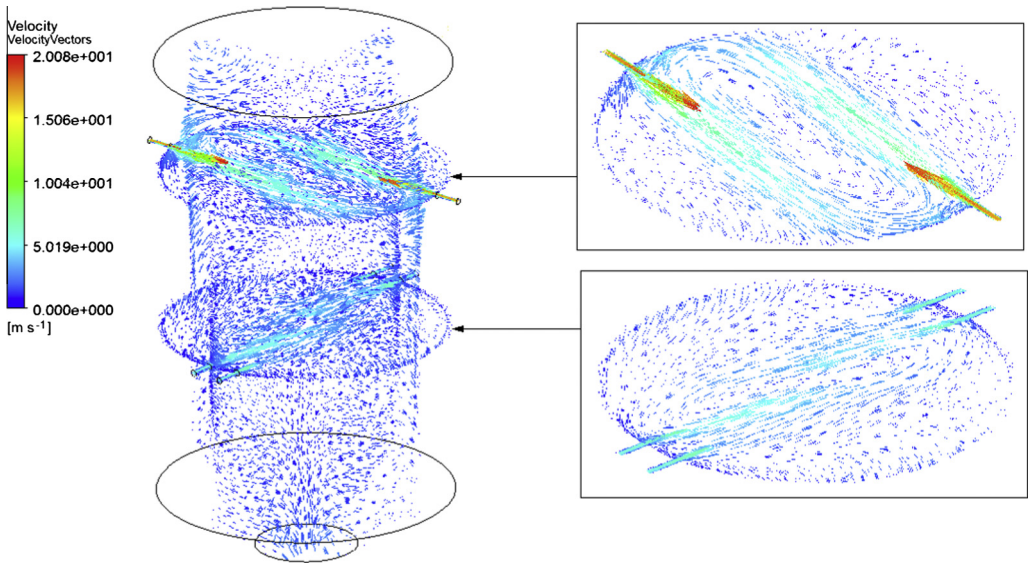

Fig. 6. The velocity vectors at the sectional planes of the gasifier (Case E) with a close view of AA′ and BB′ planes.

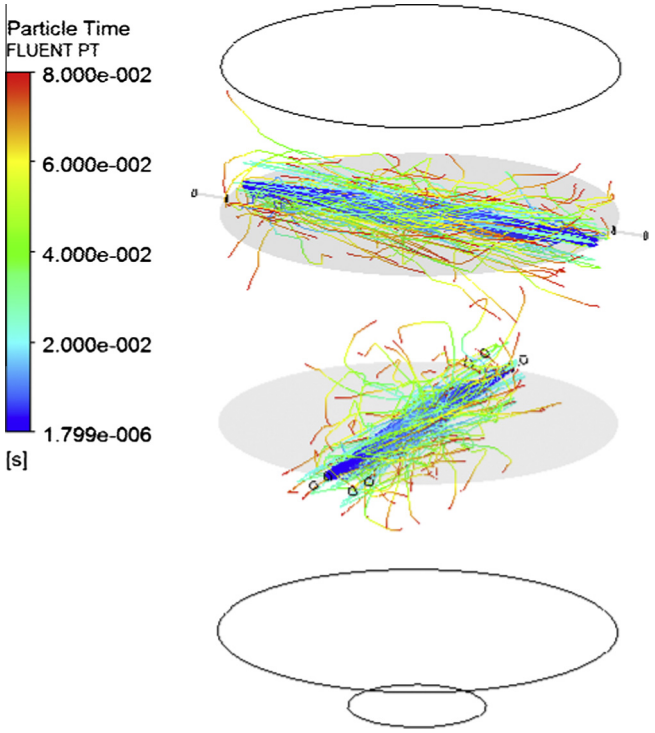

Fig. 7. The particles residence time at the sectional planes of the gasifier (Case E) (for clarity only 200 particle tracks are shown with particle end time limited at 0.8 s).

equations. For coupling the velocity and pressure, SIMPLE algorithm was followed. Convective terms were spatially discredited by second-order-upwind scheme. The values for temperature dependent properties were calculated using piecewise-polynomial equations for all gas and solid species. Convergence of the solution was achieved when the mass, turbulent kinetic energy and momentum residuals satisfied at 10^{-3} and residuals for energy and radiation at 10^{-6}. Parallel processing was used for computation. The cold flow simulations were converged first in all the cases then the reacting flows were solved by activating all reactions along with the injection of coal with ignition temperature of 2000 K.

3. Results and discussion

The effects of coal and oxidant distributions for two stages were investigated through various simulations by varying the mass fraction (%) of total coal or total oxidant at both injection levels. The overall oxygen/coal (O/C) ratio was maintained at 0.9, 1.0 and 1.1 for preliminary validation study as per available experimental condition [37]. The rest of cases were simulated through validated model at constant O/C ratio of 1.0. The names of simulation cases referred to the percentages of coal and oxygen at top level (AA′-level). Table 4 describes parameters of simulated conditions of all cases.

3.1. Selection of best reaction mechanism and validation of the model

Fig. 4 shows the comparison between the experimental results [37] and various preliminary simulation cases (Case A to F from Table 2) on the basis of mol% of CO, H_2 and CO_2. In all those cases the coal or oxygen distribution between the two stages is kept constant as per experimental conditions (Coal 50% (of total) at AA′ level and O_2 60% (of total) at AA′ level). Three O/C ratios 0.9, 1.0 and 1.1 were taken to validate the model. The temperature profiles along the axis of gasifier for all simulated cases and experimental observations are shown in Fig. 5 at different O/C ratios.

It is clear from Fig. 4 for all O/C ratio cases, that there is great impact for reaction-sets on the overall composition of syngas composition. Case A follows the most common reaction-sets i.e. the partial combustion of char and volatiles and the involvement of CO combustion in the bulk gas phase. But from Fig. 4(a–c), it shows that it predicts quite less CO and high CO_2 as compared to experimental values for this particular type of gasifier with different arrangements of injecting nozzles. The possible cause is that the well-mixed pattern of particles with gas due to impinging and tangential injection patters of fuel and oxygen. The velocity vectors and particles are shown in Figs. 6 and 7 that gives a clear idea of flow behavior of gas inside the gasifier along with the 250 collisions of particles. Fig. 7 shows the particles' residence time for 200 tracks only with limited end time i.e. 0.8 s. Fig. 7 confirms the idea that there is a greater chance to have the particle combustion as compared to CO combustion due to homogeneous temperature mixing but in case A the false unrealistic prediction is visible due to rapid CO combustion and increasing the temperature of

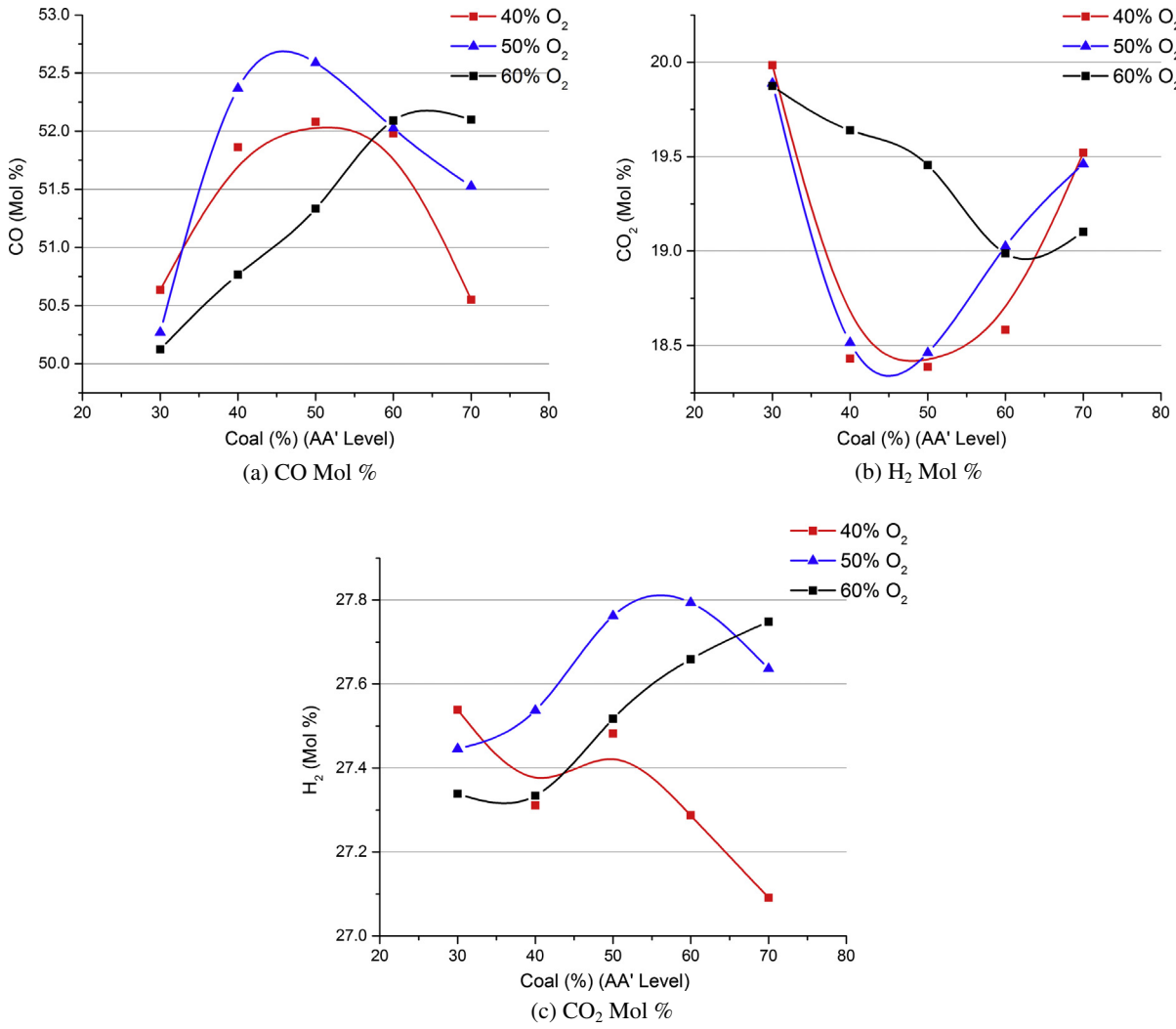

Fig. 8. The mol% for CO, H_2 and CO_2 with variation in total coal/oxygen % at AA′ level.

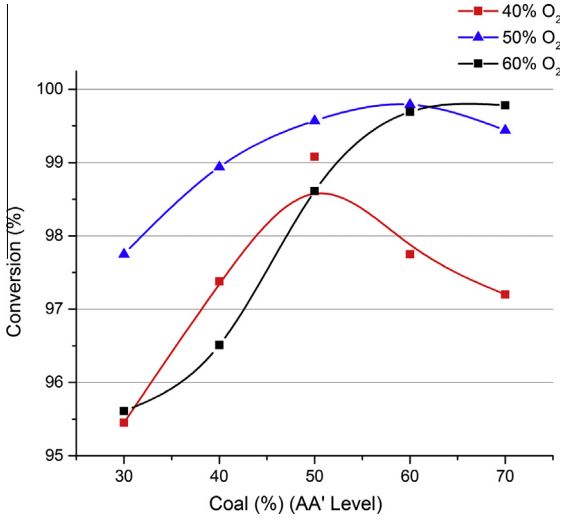

Fig. 9. The char conversion with variation in coal/oxygen % at AA′ level.

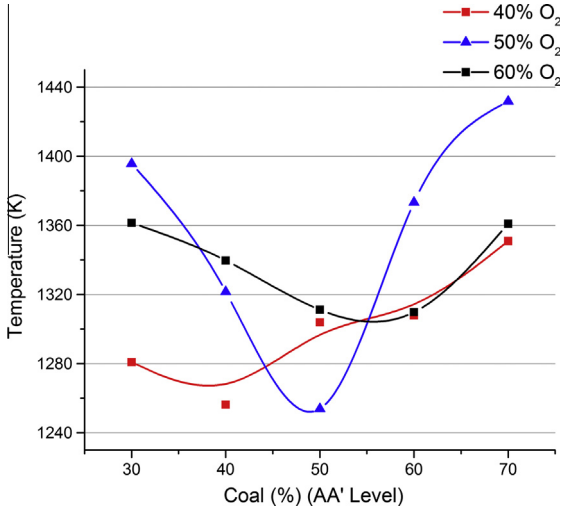

Fig. 10. Syngas average exit temperature (K).

overall gas mix. The excess temperature rise can also be verified in Fig. 5 for same case. Rest of the cases (from B to F) shows a good agreement of H_2 mol% but there are significant differences for CO and CO_2 mol%. In this regard, Case E shows the best results compared with experimental values for prediction of syngas composition and temperature at different O/C conditions. The reaction mechanism of case E contains the complete combustion of volatiles

and char and ignoring the CO combustion reaction. The values of CO and H_2 mol% for this case are in good agreement and show less than 1% error while the prediction of CO_2 is moderate but good as compared to other cases. The one reason for not predicting the good CO_2 is the assuming no formation of other species like CH_4, etc. Temperature prediction through case E is also in satisfactory limits (less than 1% error) so Case E has been validated and reaction mechanism of Case E has selected to proceed for rest of studies.

3.2. Effects of coal/oxygen distribution on syngas composition

15 Different cases were simulated at O/C ratio = 1.0 by varying coal and oxygen distribution at both the injection levels as per Table 4. The effects on the mol% of CO, CO_2 and H_2 by varying the total coal % at AA′ level are shown in Fig. 8. As per Fig. 8(a), the mol% of CO shows first increasing and then decreasing trend by increasing coal% at AA′ level with 40% and 50% oxygen at same level. This behavior is slightly changed with 60% oxygen case where it is almost of increasing order. The optimized conditions for maximum CO production (52.59%) was found at 50% coal and oxygen at AA′ level (C50_O50 case). The minimum CO mol% was observed 50.123% in C30_O60 case. Exactly inverse trends can be seen for CO_2 mol% with respective cases (Fig. 8(b)). A plausible cause for these trends is the variation of oxygen/coal ratio at local levels and the rate of mixing due to vortex formation with the tangential nozzles (either at AA′ level or BB′ level) as explained by Seo et al. [28]. The maximum and minimum for CO_2 mol% were observed 19.98% and 18.39% in C30_O60 and C50_O40 cases respectively.

The production for H_2 was found in the range of 27–28% in all the cases as per Fig. 8(c). In this narrow range (27–28%) it shows a bit increasing and then decreasing trend with increasing coal at AA′ level for 50% oxygen; a decreasing trend with 40% oxygen and almost increasing behavior with 60% at AA′ level. The reason for this behavior of H_2 production in these various cases is the non-availability of abundant water because all the gasification simulations were carried out without steam. Further there is also less moisture (1.16%) present in the coal as per its proximate analysis (refer Table 1). The less presence of water has a great influence on the water-shift reaction as per earlier studies [47,48].

3.3. Effects on char conversion

The coal/oxygen variation at both distributions has impact on its local ratio distribution and that has also impact on the overall char conversion. This impact is shown in Fig. 9 for various simulated cases. In general an increase can be seen in conversion by increasing the coal at top level (from 30% to 50%) with all oxygen cases. But conversion decreases by increasing coal from 50% to 70% at top level (AA′) with 40% oxygen at that level. The other two conditions (50% and 60% oxygen at top) show a continual increase in conversion by increasing coal from 50% to 70%. This behavior is due to greater residence time of the coal injected at top-level (AA′ level) as compared to the coal injected at bottom level (BB′ level) according to the conclusions of earlier studies [18,49]. So the higher amount of coal injected at AA′ level with sufficient oxygen has enough residence time to reach at maximum conversion, usually more than 99%. The minimum char conversion

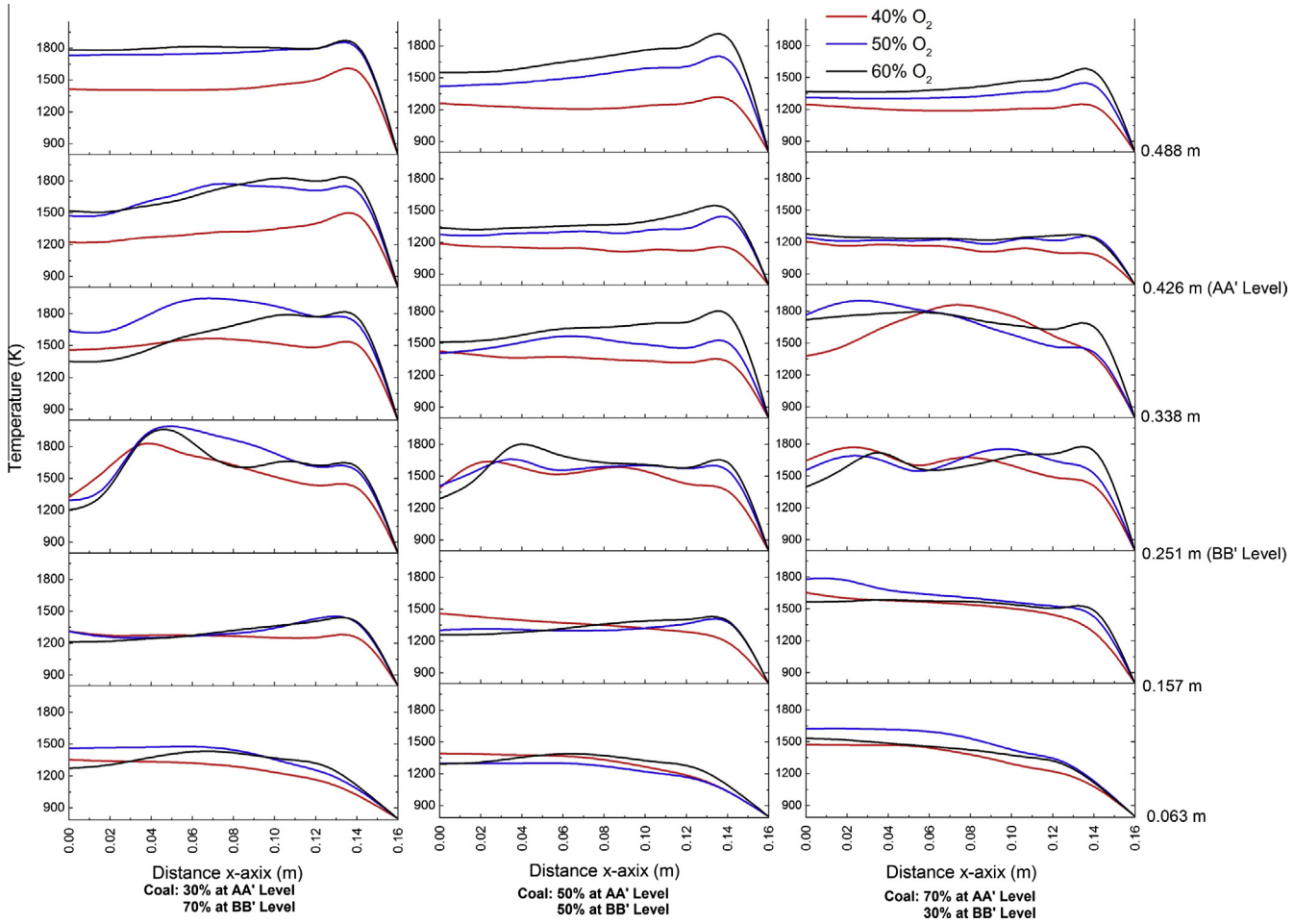

Fig. 11. Radial temperature profiles for various simulation cases at different heights of gasifier.

i.e., 95.45% was found with 30% coal and 40% oxygen at top level case (C30_O40) whereas the maximum char conversion was found 99.7% in C60_O50 and C70_O60 both the cases.

3.4. Effects on syngas exit temperature and maximum inside temperature

The temperature plays an important role in the gasification system. The variations in the coal and oxygen at both the injection levels actually affect local oxygen/coal ratio as discussed in previous sections and hence the defined combustion/gasification reactions occurred with different rates. Because of the difference of those exothermic and endothermic reaction rates there is an increase or decrease in the overall temperatures. Fig. 10 shows an overall picture for the syngas exit temperatures for simulated cases. It is clear that in all the cases the exit temperature for syngas is in the range from 1250 K to 1450 K. Li et al. [34] observed that in the center of impinging zone there is an increase of particle cohesion and agglomeration by resulting a high particle concentration region. The rapid deceleration of particles near the center of

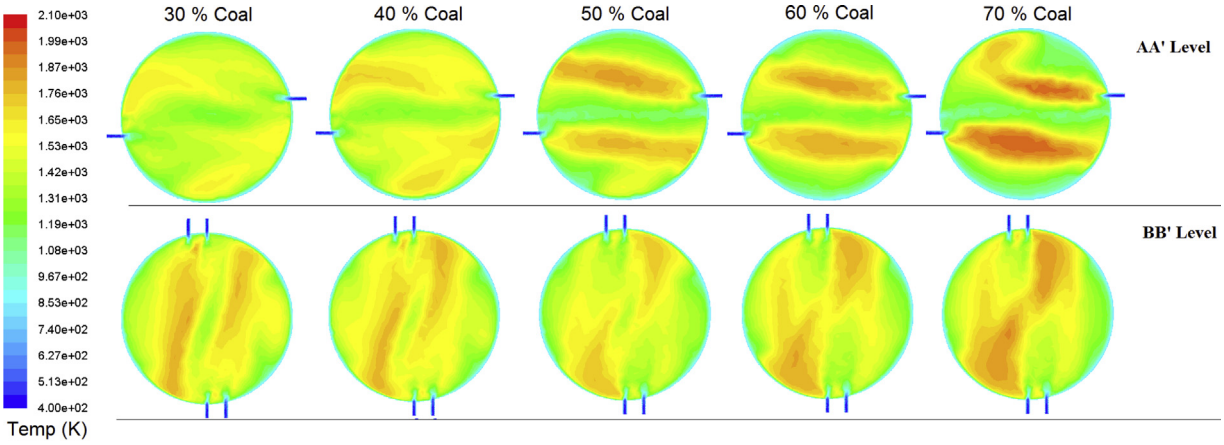

(a) 40% Oxygen at AA' Level

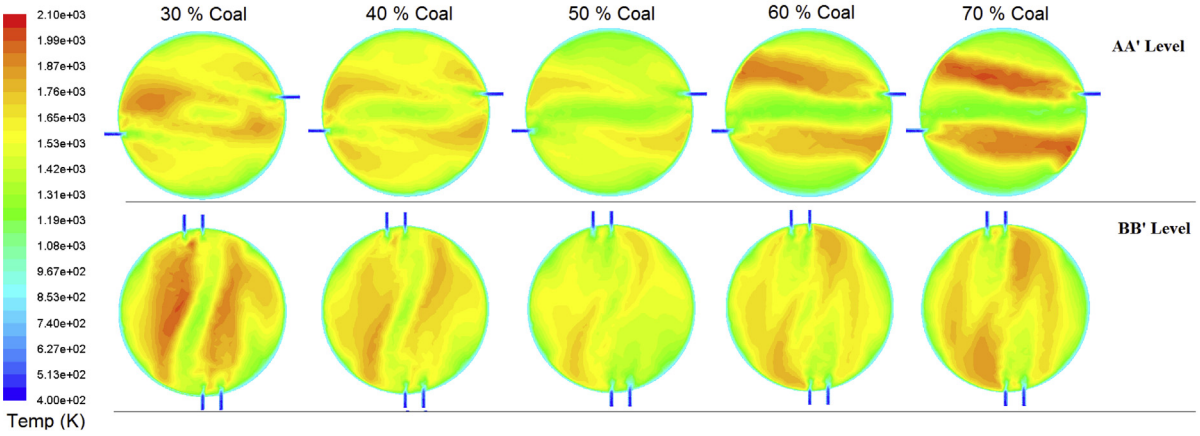

(b) 50% Oxygen at AA' Level

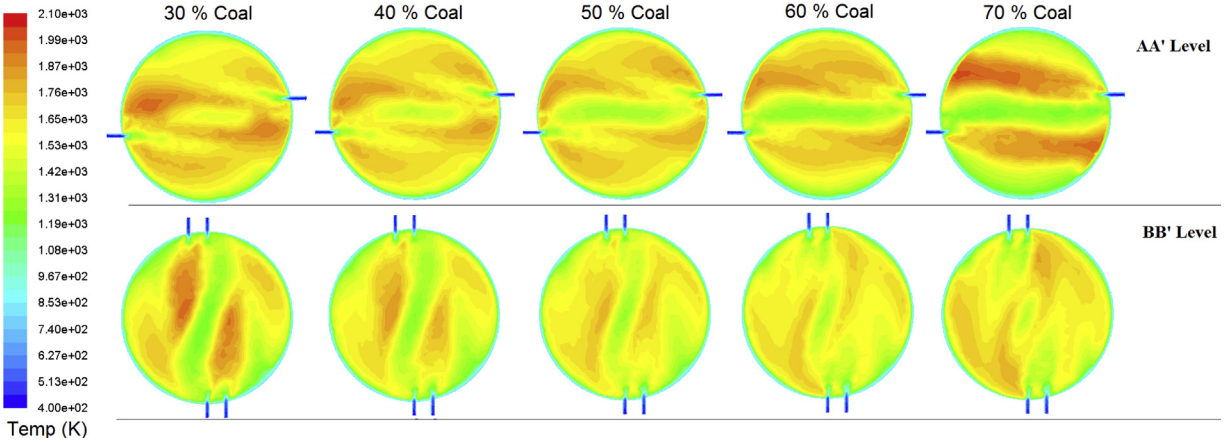

(c) 60% Oxygen at AA' Level

Fig. 12. Temperature contours for sectional planes at AA′ level and BB′ level.

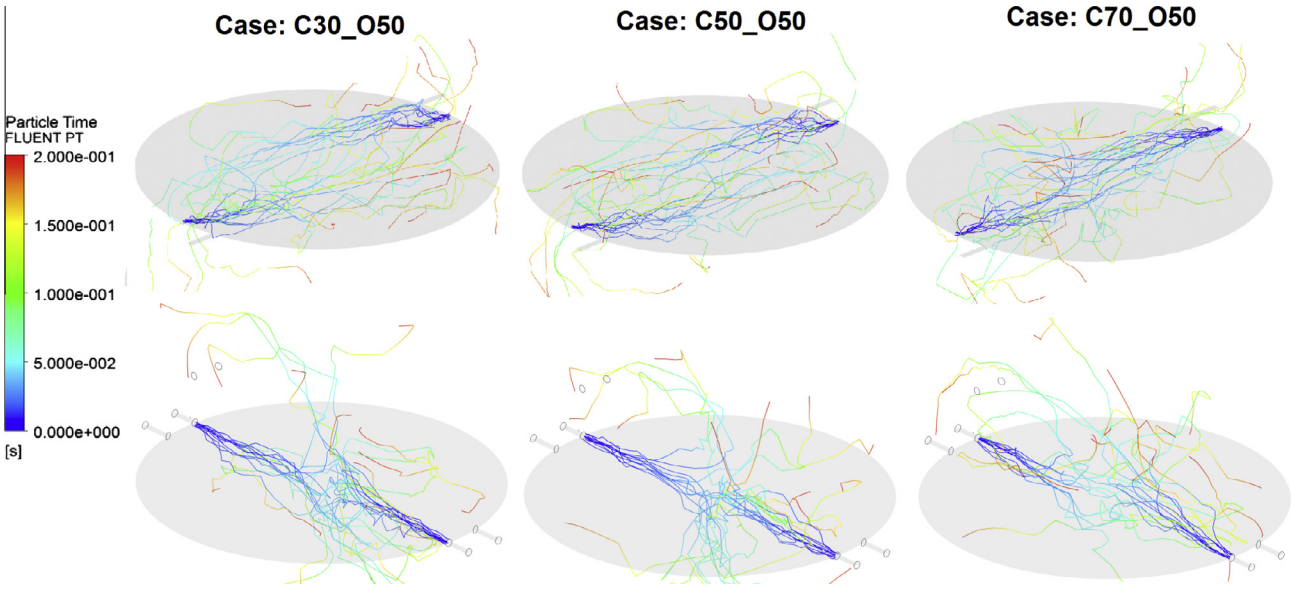

Fig. 13. The particles residence time at the sectional planes of the gasifier; Cases: C30_O50, C50_O50 and C70_O50 (for clarity only 20 particle tracks are shown with particle end time limited at 0.2 s).

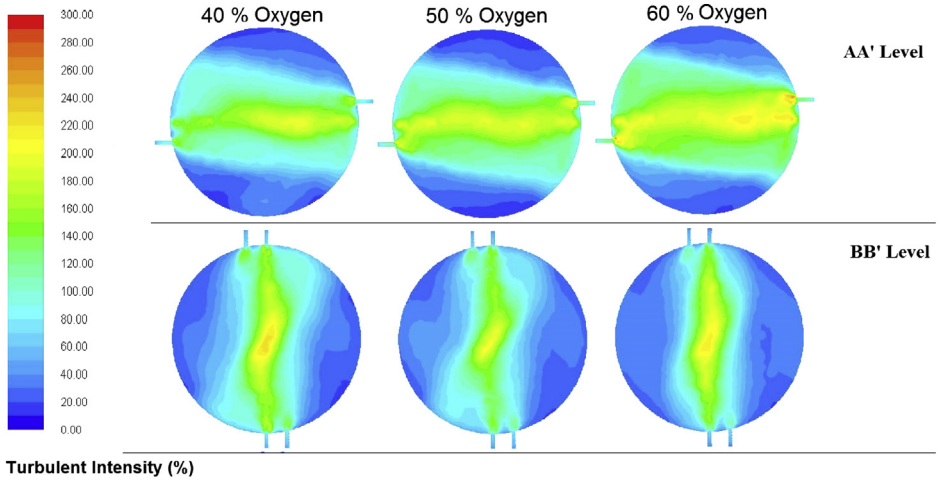

(a) at constant 50% coal at both injection levels

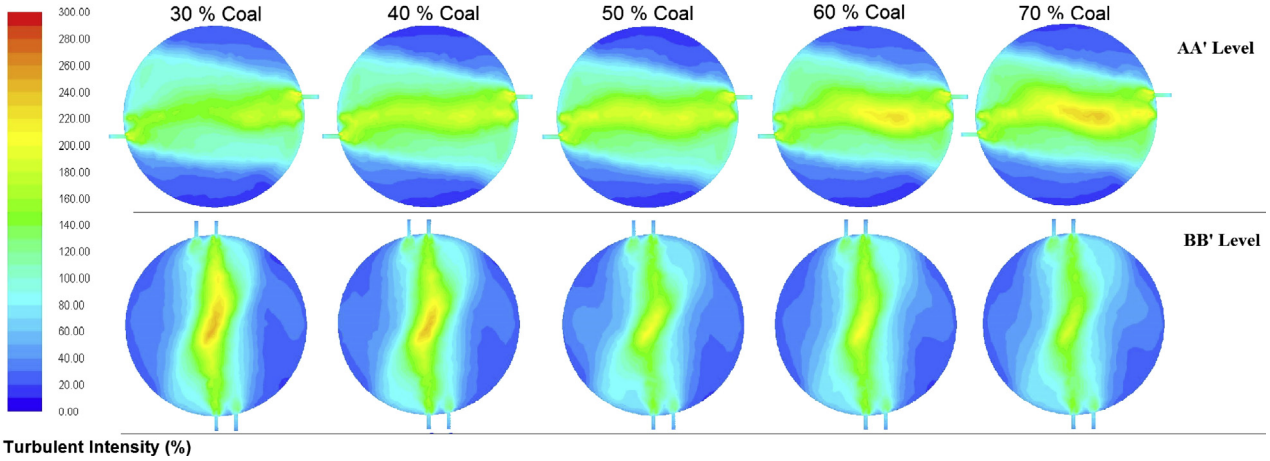

(b) at constant 50% Oxygen at both injection levels

Fig. 14. Turbulent intensity (%) contours for selected cases.

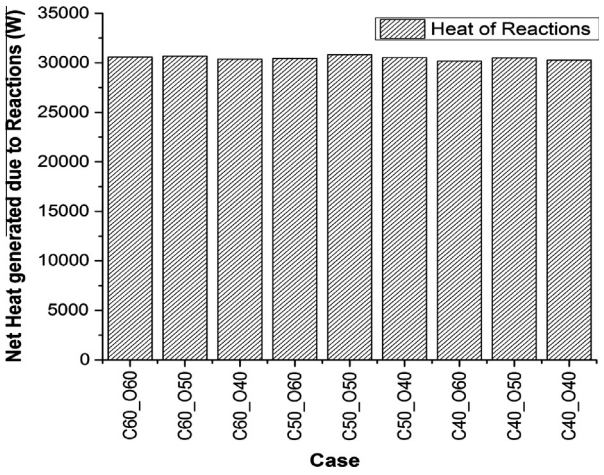

Fig. 15. Net heat generated due to reactions (W) for selected cases.

impinging zone improves the performance of gasifier in terms of heat and mass transfer.

The radial temperature profiles from center can be seen in Fig. 11 for three coal distribution scenarios. It is evident that there is great impact for the local temperature distribution due to variation in coal or oxidant between two stages. Further the results can be verified by examining the temperature profile contours of top and bottom injection sectional planes as given in Fig. 12.

It is apparent from those temperature contours that the inside temperature increases by increasing the amount of coal at any level with appropriate amount of oxygen. The maximum temperature was observed 2027 K at AA′ level with 70% of total coal and 60% of total oxygen (Case C70_O60, Fig. 12(c)).

3.5. Effects of coal distribution on particle trajectories

The particle residence time is key parameters for the conversion of char and occurrence of different reactions with their specific rates, as explained in earlier section. The effects on the particle residence time can be depicted from Fig. 13, where particles trajectories are shown for variation of coal distribution with fixed 50% oxygen distribution at both the levels. For clarity the trajectories are limited to 20 particle streams with maximum 0.2 s. The variation in coal at any injection level with fixed oxygen actually impacted on the local particle/gas volume ratio and hence ultimately impacted on the particle trajectories. It is observed that the less particle/gas ratio increases the particles residence time and confirms the previous studies [44].

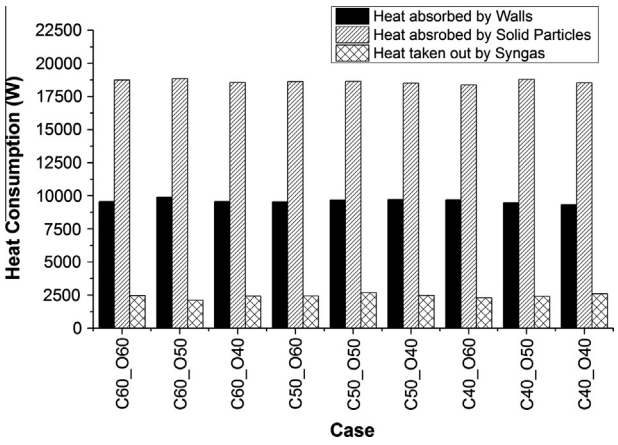

Fig. 16. Heat consumption in different ways.

3.6. Effects on turbulent intensity

Turbulent intensity has predicted by solving the equations of reliable k–ε model from Eqs. (5)–(9). Due to impinging and tangential nozzles at AA′ and BB′ levels, the major turbulence has observed on the sectional planes on these levels. The effects of coal and oxygen distribution on Turbulent Intensity can be visualized from Fig. 14. The turbulent intensity of 108–300% has observed at the main reaction zone on both the planes. The obvious reason is the high mixing rate at these sectional planes for injectors.

3.7. Heat generation and consumption analysis

The overall energy balances accounted through Eq. (3). The primary source for generation of heat energy is from exothermic reactions. Then the heat is consumed by endothermic reactions and remaining heat is either absorbed by walls which are assumed to be at constant temperature of 800 K (water cooled system) or taken out with syngas. A fraction of heat is also consumed by the solid fuel particles to raise their temperature for drying, devolatilization and then reactions. The net heat generated through reactions has observed in the range of 3000 W and shown in Fig. 15 for few selected cases. The maximum heat consumed by the solid fuel particles and observed in the range of 18,700 W (Fig. 15). Heat lost through walls is found in the range of 9000 W whereas the heat carried away by syngas is found in 2000–26,000 W (Fig. 16).

4. Conclusion

Double-stage entrained flow gasifier with multi opposite burners for lignite coal has numerically simulated through commercial CFD software in present study. The fuel feeding injectors were impinging and tangential in nature to produce slightly vortex flow inside the gasifier. In the first part different reaction mechanisms were simulated as per experimental conditions. After the validation of model with one best reaction mechanism, further investigations were made to study the effects of coal and oxygen distributions between the two feeding injection levels. As per preliminary simulations, it was concluded that:

- The complete combustion of char and volatiles reaction mechanism can predict the mol% of CO, H_2 and CO_2 with less than 1% error.
- The variation of oxygen or coal at any injection level basically impacted on the local oxygen/coal ratio and the gas–solid mixing pattern. This impact is transferred in the variation of char consumption rates with combustion and gasification reactions and that plays a key role in the variation of syngas components and temperature.
- A little variation was seen in H_2 mol% by changing coal or oxygen at both the levels due to very less moisture in the coal along with the consideration of non-steam gasification. The production for H_2 was found in the range of 27–28 mol% in all the cases. The maximum CO mol% was found 52.59% for 50% coal and 50% oxygen at upper injection level (AA′) whereas the minimum CO mol% was observed 22.37% for 30% coal and 70% oxygen at upper level (AA′). The maximum and minimum for CO_2 mol% were observed 47.86% and 18.39% in 30% coal with 70% oxygen and 50% coal with 40% oxygen at AA′ level respectively.
- The exit temperature for syngas was found in the range from 1250 K to 1450 K. The maximum temperature was observed 2027 K at AA′ level with 30% of total coal and 70% of total oxygen at upper injection level.
- The maximum char conversion was found 99.79% with coal 60% and oxygen 50% of total at AA′ level. The minimum char conversion was observed 95.45% at 30% coal with 40% oxygen at AA′ level.

- The maximum turbulent intensity has observed 300% at the main reaction zone on both injecting planes due to high mixing rate at these sectional planes for injectors.
- In general with oxygen/coal above or equal to 50% of total at upper injection level has shown an optimized performance.

Overall it was concluded that the coal and oxygen distribution has great effect on the syngas composition, char conversion and exit syngas temperature. The temperature and kinetics of gasification reactions (reactions of char to CO_2 and H_2O) can be controlled with the optimized coal and oxidant distribution between the two stages. These parameters are critical to the overall performance of the gasifier, so coal and oxygen feedings must be optimized between the two stages of the gasifier to get the optimized performance.

Acknowledgments

The present work is a part of ongoing research project INSPIRE funded by HEC Pakistan. The project is being conducted with mutual collaboration between Mehran University of Engineering & Technology Jamshoro Pakistan and Shenyang Aerospace University China. The Chinese professors are highly acknowledged for their proper technical and CFD guidance.

References

[1] Akikur R, Saidur R, Ping H, Ullah K. Performance analysis of a co-generation system using solar energy and SOFC technology. Energy Convers Manage 2014;79:415–30.
[2] Carapellucci R, Saia R, Giordano L. Study of gas-steam combined cycle power plants integrated with MCFC for carbon dioxide capture. Energy Proc 2014;45:1155–64.
[3] RAO A. Gas-fired combined-cycle power plant design and technology. Adv Power Plant Mater Des Technol 2010;32:32–53.
[4] Cau G, Cocco D, Serra F. Energy and cost analysis of small-size integrated coal gasification and syngas storage power plants. Energy Convers Manage 2012;56:121–9.
[5] Silaen A, Wang T. Effect of turbulence and devolatilization models on coal gasification simulation in an entrained-flow gasifier. Int J Heat Mass Transfer 2010;53:2074–91.
[6] Vicente W, Ochoa S, Aguillón J, Barrios E. An Eulerian model for the simulation of an entrained flow coal gasifier. Appl Therm Eng 2003;23:1993–2008.
[7] Chen C, Horio M, Kojima T. Use of numerical modeling in the design and scale-up of entrained flow coal gasifiers. Fuel 2001;80:1513–23.
[8] Tominaga H, Yamashita T, Ando T, Asahiro N. Simulator development of entrained flow coal gas-ifiers at high temperature and high pressure atmosphere. IFRF Combust J 2000;1–22. <http://www.journal.ifrf.net/library/-(2000,04,Tominaga)>.
[9] Jian-ping ZJ-hK, Jian-zhong ZZ-jL, Ke-fa C. Numerical simulation for pulverized coal gasifier's fluid flow characteristic on cold and hot condition. Proc CSEE 2007;27:30–5.
[10] Wu Y-X, Zhang J-S, Yue G-X, Lü J-F. Analysis of the gasification performance of a staged entrained flow gasifier by presumed PDF model. J Chem Ind Eng (China) 2008;28:29–34.
[11] Andries J, Becht J, Hoppesteyn P. Pressurized fluidized bed combustion and gasification of coal using flue gas recirculation and oxygen injection. Energy Convers Manage 1997;38:S117–22.
[12] Nguyen TD, Ngo SI, Lim Y-I, Lee JW, Lee U-D, Song B-H. Three-stage steady-state model for biomass gasification in a dual circulating fluidized-bed. Energy Convers Manage 2012;54:100–12.
[13] Gerun L, Paraschiv M, Vijeu R, Bellettre J, Tazerout M, Gøbel B, et al. Numerical investigation of the partial oxidation in a two-stage downdraft gasifier. Fuel 2008;87:1383–93.
[14] Bouma P, de Goey L, Tummers M, Kiel J. Numerical modelling of an entrained-flow gasification simulator. ASME Press Vess Pip Div Publ PVP 1999;397:227–35.
[15] Guenther C, Breault R. The effect of gas–solids dispersion on a two fluid model of a transport gasifier. In: AIChE annual meeting and fall showcase, Cincinnati, OH; October 30–November-4, 2005.
[16] Álvarez L, Gharebaghi M, Jones J, Pourkashanian M, Williams A, Riaza J, et al. Numerical investigation of NO emissions from an entrained flow reactor under oxy-coal conditions. Fuel Process Technol 2012;93:53–64.
[17] Choi YC, Li XY, Park TJ, Kim J, Lee J. Numerical study on the coal gasification characteristics in an entrained flow coal gasifier. Fuel 2001;80:2193–201.
[18] Watanabe H, Otaka M. Numerical simulation of coal gasification in entrained flow coal gasifier. Fuel 2006;85:1935–43.
[19] Fletcher D, Haynes B, Christo F, Joseph S. A CFD based combustion model of an entrained flow biomass gasifier. Appl Math Model 2000;24:165–82.
[20] Ajilkumar A, Sundararajan T, Shet U. Numerical modeling of a steam-assisted tubular coal gasifier. Int J Therm Sci 2009;48:308–21.
[21] Md Saiful A, Wijayanta AT, Nakaso K. Predictions of O_2/N_2 and O_2/CO_2 mixture effects during coal combustion using probability density function. J Novel Carbon Resour Sci 2010;2:12–6.
[22] Dong C, Yang Y, Yang R, Zhang J. Numerical modeling of the gasification based biomass co-firing in a 600 MW pulverized coal boiler. Appl Energy 2010;87:2834–8.
[23] Silaen A, Wang T. Investigation of the coal gasification process under various operating conditions inside a two-stage entrained flow gasifier. J Therm Sci Eng Appl 2012;4:021006.
[24] Talab I, Al-Nahari Z, Qudaih R, Janajreh I. Numerical modeling of coal tire-shred co-gasification. JJMIE 2010;4:155–62.
[25] Chui E, Majeski A, Lu D, Hughes R, Gao H, McCalden D, et al. Simulation of entrained flow coal gasification. Energy Proc 2009;1:503–9.
[26] Slezak A, Kuhlman JM, Shadle LJ, Spenik J, Shi S. CFD simulation of entrained-flow coal gasification: coal particle density/size fraction effects. Powder Technol 2010;203:98–108.
[27] Kong X, Zhong W, Du W, Qian F. Compartment modeling of coal gasification in an entrained flow gasifier: a study on the influence of operating conditions. Energy Convers Manage 2014;82:202–11.
[28] Seo H-K, Park S, Lee J, Kim M, Chung S-W, Chung J-H, et al. Effects of operating factors in the coal gasification reaction. Korean J Chem Eng 2011;28:1851–8.
[29] Du S-W, Chen W-H, Lucas J. Performances of pulverized coal injection in blowpipe and tuyere at various operational conditions. Energy Convers Manage 2007;48:2069–76.
[30] Singer S, Chen L, Ghoniem AF. The influence of gasification reactions on char consumption under oxy-combustion conditions: effects of particle trajectory and conversion. Proc Combust Inst 2013;34:3471–8.
[31] Chen C-J, Hung C-I, Chen W-H. Numerical investigation on performance of coal gasification under various injection patterns in an entrained flow gasifier. Appl Energy 2012;100:218–28.
[32] Zheng L, Furinsky E. Comparison of Shell, Texaco, BGL and KRW gasifiers as part of IGCC plant computer simulations. Energy Convers Manage 2005;46:1767–79.
[33] Ni J, Liang Q, Zhou Z, Dai Z, Yu G. Numerical and experimental investigations on gas-particle flow behaviors of the opposed multi-burner gasifier. Energy Convers Manage 2009;50:3035–44.
[34] Li C, Dai Z, Li W, Xu J, Wang F. 3D numerical study of particle flow behavior in the impinging zone of an opposed multi-burner gasifier. Powder Technol 2012;225:118–23.
[35] Dai Z, Gong X, Guo X, Liu H, Wang F, Yu Z. Pilot-trial and modeling of a new type of pressurized entrained-flow pulverized coal gasification technology. Fuel 2008;87:2304–13.
[36] Tang Z, Ma P, Li Y-L, Tang C, Xing X, Lin Q. Design and experiment research of a novel pulverized coal gasifier based on flameless oxidation technology. Proc CSEE 2010;30:50–5 [in Chinese].
[37] Tang Z, Ma P, Yu Y, Li Y-L, Xing X, Lin Q. Numerical simulation of a new two-stage dry feed gasifier for double-high coal. J China Coal Soc 2010;35:481–5 [in Chinese].
[38] Jones W, Launder B. The prediction of laminarization with a two-equation model of turbulence. Int J Heat Mass Transfer 1972;15:301–14.
[39] Launder BE, Spalding D. The numerical computation of turbulent flows. Comput Methods Appl Mech Eng 1974;3:269–89.
[40] Gonzalo-Tirado C, Jiménez S, Ballester J. Gasification of a pulverized sub-bituminous coal in CO_2 at atmospheric pressure in an entrained flow reactor. Combust Flame 2012;159:385–95.
[41] Fluent I. ANSYS FLUENT 14: theory guide. USA: Fluent Inc.; 2012.
[42] Chen W-H, Du S-W, Yang T-H. Volatile release and particle formation characteristics of injected pulverized coal in blast furnaces. Energy Convers Manage 2007;48:2025–33.
[43] Wen C, Chaung T. Entrainment coal gasification modeling. Ind Eng Chem Process Des Develop 1979;18:684–95.
[44] Steiler JM, Lao D, Lebonvallet JL. Development of coal injection in the blast furnace at Usinor Sacilor. Inject Technol Iron Mak Steel Mak Proc 1996:15–32.
[45] Du S-W, Chen W-H. Numerical prediction and practical improvement of pulverized coal combustion in blast furnace. Int Commun Heat Mass Transfer 2006;33:327–34.
[46] Ubhayakar SK, Stickler DB. Rapid devolatilization of pulverized coal in hot combustion gases. In: Symposium (international) on combustion. Elsevier; 1977. p. 427–36.
[47] Lu X, Wang T. Water–gas shift modeling in coal gasification in an entrained-flow gasifier. Part 1: development of methodology and model calibration. Fuel 2013;108:629–38.
[48] Lu X, Wang T. Water–gas shift modeling in coal gasification in an entrained-flow gasifier–Part 2: gasification application. Fuel 2013;108:620–8.
[49] Guo X, Dai Z, Gong X, Chen X, Liu H, Wang F, et al. Performance of an entrained-flow gasification technology of pulverized coal in pilot-scale plant. Fuel Process Technol 2007;88:451–9.